Chemical Science

ROYAL SOCIETY OF CHEMISTRY

EDGE ARTICLE

View Article Online
View Journal | View Issue

Cite this: *Chem. Sci.*, 2025, **16**, 5142

All publication charges for this article have been paid for by the Royal Society of Chemistry

Azolium-2-dithiocarboxylates as redox active ligands in nickel chemistry†‡

Martin S. Luff, [a] Tin M. Filipovic,[a] Celine S. Corsei,[a] Kai Oppel, [a] Ivo Krummenacher, [ab] Rüdiger Bertermann, [ab] Maik Finze, [ab] Holger Braunschweig [ab] and Udo Radius *[a]

The coordination chemistry of carbene-CS_2 adducts of selected NHCs and cAACs and their redox active nature in nickel complexes is reported. These azolium-2-dithiocarboxylate ligands can be considered as 1,1-isomeric dithiolene analogues bearing a 2π electron reservoir. Depending on the co-ligands attached to nickel, square planar mono- or bis-(carbene-CS_2) complexes of the types [Ni(I^iPr)$_2$(carbene-CS_2)] (**2a–g**) (carbene = $cAAC^{Me}$, IDipp, IMes, BIMe, BI^iPr, I^iPr, and I^iPr^{Me}) and [Ni(carbene-CS_2)$_2$] (**3a–c**) (carbene = $cAAC^{Me}$, IDipp, and IMes) are accessible by alkene substitution using [Ni(I^iPr)$_2$(η^2-C_2H_4)] or [Ni(COD)$_2$] as the starting material ($cAAC^{Me}$ = 1-(2,6-di-iso-propylphenyl)-3,3,5,5-tetramethylpyrrolidin-2-ylidene, IR = 1,3-diorganylimidazolin-2-ylidene, IR^{Me} = 1,3-diorganyl-4,5-dimethylimidazolin-2-ylidene, and BIR = 1,3-diorganylbenzimidazolin-2-ylidene). In the complexes **2a–g** and **3a–c**, all carbene-CS_2 ligands are coordinated in a κ^2-*S*,*S*′ fashion to nickel(II) and are ligated either in their formally one electron reduced (**3a–c**) or two electron reduced (**2a–g**) redox states. The complexes **3a–c** reveal intense NIR absorptions, which shift upon metallic reduction to the nickelate salts of the type $[Cat]^+[Ni(carbene\text{-}CS_2)_2]^{\bullet-}$ (**4a–b^{cat}**). In these nickelates, an additional electron is shared across a ligand-centered SOMO of π-symmetry which is delocalized over both azolium-2-dithiocarboxylate ligands and results in carbene-CS_2 moieties with a formal −1.5 charge per ligand, further demonstrating the flexible redox active nature of these azolium-2-dithiocarboxylate ligands.

Received 13th December 2024
Accepted 7th February 2025

DOI: 10.1039/d4sc08449g

rsc.li/chemical-science

Introduction

Redox active ligands can adopt different oxidation states upon coordination and can act as electron reservoirs for transition metal and main group elements. Therefore they have become a very important class of ligands over the last few decades.[1] Redox active ligands allow access to a plethora of different oxidation or spin states in their complexes.[2] The use of such ligands which behave as electron reservoirs with reversible redox activity and which can donate or accept one or more electrons on demand during a catalytic cycle has emerged as a powerful tool in catalysis. Such "actor ligands" can extend the electronic flexibility of the central element and directly participate in crucial bond breaking or bond forming steps, thus acting as metal–ligand bifunctional catalysts. The implementation of such metal–ligand cooperation strategies for the design of functional catalysts has been very successful in recent years. Thus, a broad variety of interesting applications of these ligands have been developed, ranging from stabilization of subvalent main group compounds[1g,3] to inexpensive 3d transition metal based complexes which mimic the catalytic activity of efficient noble metal catalysts.[1b,4] Furthermore, redox active ligands are essential components in artificial photosynthetic,[5] photoredox,[6] and electrocatalytic systems[7] as well as in heteroatom based diradicaloids.[8] Employed in these processes are mainly a broad variety of easily tunable, functionalized nitrogen or oxygen containing π-conjugated systems such as catecholates, 2,2′-bipyridines, *ortho*-amidophenolates or diazabutadienes.[3]

One of the prominent examples of such redox active ligands is sulfur-based dithiolenes, which have been a subject of interest since the 1960s as components in, for example, prototypical homoleptic square planar or trigonal prismatic transition metal complexes with interesting bonding situations.[9] In these types of compounds, the formal oxidation state of the central metal atom may not always be unambiguously determined, thus rendering them redox non-innocent.[10] For example, in square planar bis-1,2-dithiolene group 10 complexes, the central metal atom M may formally exist in

[a]*Institute for Inorganic Chemistry, Julius-Maximilians-Universität Würzburg, Am Hubland, 97074 Würzburg, Germany. E-mail: u.radius@uni-wuerzburg.de*

[b]*Institute for Sustainable Chemistry & Catalysis with Boron, Julius-Maximilians-Universität Würzburg, Am Hubland, 97074 Würzburg, Germany*

† Dedicated to Prof. Dr Franc Meyer and Prof. Dr Christian Limberg on the occasion of their 60th birthday.

‡ Electronic supplementary information (ESI) available. CCDC 2409878–2409888. For ESI and crystallographic data in CIF or other electronic format see DOI: https://doi.org/10.1039/d4sc08449g

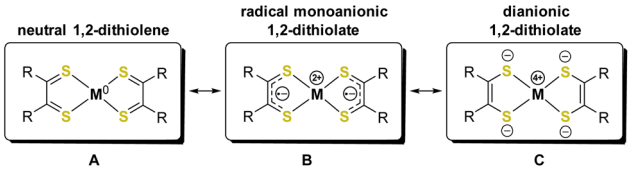

Scheme 1 Square planar group 10 bis-1,2-dithiolene complexes (M = Ni, Pd, Pt) in three possible resonance structures: A, B and C.

oxidation states 0 (**A**), +II (**B**), or + IV (**C**) (Scheme 1), as both attached 1,2-dithiolene ligands may exist in three possible redox states: a regular neutral 1,2-dithiolene (**A**), a radical monoanionic form (**B**), or a dianionic 1,2-dithiolate ligand (**C**).

This mesomeric flexibility, *i.e.*, the redox active nature, of dithiolenes often leads to unique physical properties.[11] For example, group 10 bis-dithiolene complexes, especially those of nickel, have attracted considerable interest for application as switchable, modulable near-infrared (NIR) dyes for medicinal and technical purposes.[12] Due to the synthetic availability of the ligands, the majority of known group 10 bis-dithiolene systems are mostly limited to the 1,2-substitutional pattern with just a few examples known for related 1,1-isomeric dithiolate complexes.[13]

An interesting class of molecules in this respect includes 1,1-dithiolene analogues derived from Lewis-acid–base adducts of N-heterocyclic carbenes (NHCs) or cyclic (alkyl)(amino)carbenes (cAACs) with CS_2, which form zwitterionic azolium-2-dithiocarboxylates (*vide infra*, Schemes 2 and 3).[14] Although these compounds have been used as ligands in transition metal chemistry before,[14b,k,15] they have so far not been considered for the synthesis of bis-dithiolene nickel complexes. Just recently we reported that NHC- and cAAC-based neutral carbene-CS_2 adducts (**A**), *i.e.*, azolium-2-dithiocarboxylates, undergo reductive complexation with metallic main group reductants to yield magnesium or potassium complexes of radical-anions [carbene-CS_2]$^{\cdot-}$ (**B**).[16] Furthermore, earlier studies have also reported the synthesis of alkali metal clusters of dianions of the type [carbene-CS_2]$^{2-}$ (**C**),[17] demonstrating that the π-system of carbene-CS_2 adducts may act as a π-electron reservoir for up to two added electrons (Scheme 2). Despite these interesting properties, reports on the redox activity of azolium-2-dithiocarboxylates as ligands are limited to two very recent studies.[15s,t]

Considering the significance of such redox active complexes in materials science and catalysis we were interested in developing azolium-2-dithiocarboxylate nickel chemistry based on NHCs and cAACs. We herein report the synthesis and characterization of several azolium-2-dithiocarboxylate nickel complexes, thereby clearly demonstrating the redox active nature of this class of ligands.

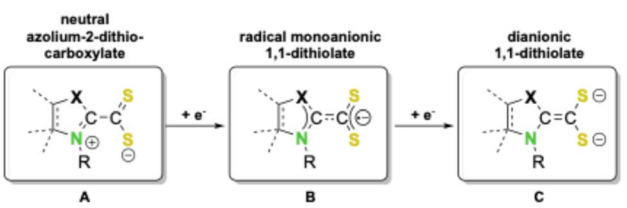

Scheme 2 Three redox-states of azolium-2-dithiocarboxylates (X = CMe_2, NR).

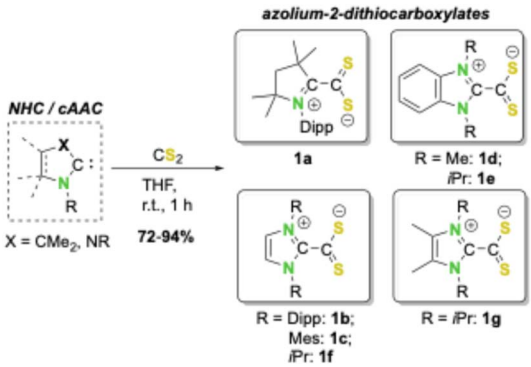

Scheme 3 Synthesis of azolium-2-dithiocarboxylates **1a–g**.[14d,g–j,16]

Results and discussion

We started our study with the synthesis of different carbene-CS_2 adducts of a set of electronically and sterically different N-heterocyclic carbenes (NHCs), such as the cAAC-based adduct $cAAC^{Me}$-CS_2 (**1a**; $cAAC^{Me}$ = 1-(2,6-di-iso-propylphenyl)-3,3,5,5-tetramethylpyrrolidin-2-ylidene), several *N*-aryl substituted NHC-adducts such as IDipp-CS_2 (**1b**) and IMes-CS_2 (**1c**; IR = 1,3-diorganylimidazolin-2-ylidene), π-benzannulated adducts such as BIMe-CS_2 (**1d**) and BI^{i}Pr-CS_2 (**1e**: BIR = 1,3-diorganylbenzimidazolin-2-ylidene), and nitrogen and/or backbone alkylated carbene-CS_2 adducts such as I^{i}Pr-CS_2 (**1f**) and I^{i}Pr^{Me}-CS_2 (**1g**; IR^{Me} = 1,3-diorganyl-4,5-dimethylimidazolin-2-ylidene). These NHC-CS_2 adducts can be synthesized in large quantities and high yields from the reaction of CS_2 and the free NHC (see Scheme 3), as reported previously for most of these azolium-2-dithiocarboxylates.[14d,g–j,16] As the synthesis of BI^{i}Pr-CS_2 (**1e**) is unknown we present the synthesis and characterization of this compound in the ESI.‡ [18] Recently, we also presented the detailed redox chemistry and the electronic properties of many of these azolium-2-dithiocarboxylates, which typically feature quasi-reversible redox events. These redox waves correspond to the reduction to either radical monoanions ([NHC-CS_2]$^{\cdot-}$) or dianions ([carbene-CS_2]$^{2-}$) (for an overview of the cyclic voltammograms recorded for **1a–g** see Fig. S1 of the ESI‡).[16]

Due to our long-standing interest in nickel chemistry,[19] we were interested in the reductive coordination of these neutral carbene-CS_2 ligands with suitable electron-rich nickel(0) precursors.[20] Therefore, we chose [Ni(I^{i}Pr)$_2$(η^2-C_2H_4)][20a] as the starting material, as it provides access to the reactive, coordinatively unsaturated complex {Ni(I^{i}Pr)$_2$}.[19,20] Solutions of [Ni(I^{i}Pr)$_2$(η^2-C_2H_4)] in toluene react immediately with azolium-2-dithiocarboxylates **1a–g** accompanied by a color change from orange to yellow (**2a–c**) or green (**2d–g**) (see Scheme 4).

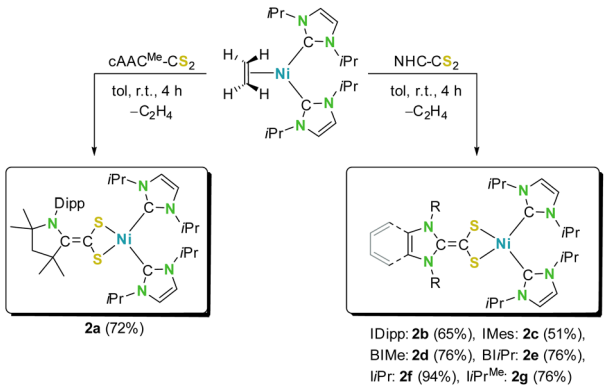

Scheme 4 Synthesis of mono-azolium-2-dithiocarboxylate nickel complexes of the type [Ni(I^{i}Pr)$_2$(carbene-CS$_2$)] (**2**).

Depending on the nature of the carbene-CS$_2$ adduct used, the resulting products of these reactions either precipitated (**2f–g**) over several hours from these solutions or remained entirely (**2a–c**) or partially (**2d–e**) in solution. Workup led to the isolation of the complexes [Ni(I^{i}Pr)$_2$(carbene-CS$_2$)] (**2a–g**) in 51–94% yield (Scheme 4). Although NMR scale synthesis of **2a–g** indicated quantitative formation of the products, isolation on a preparative scale in high purity afforded lower yields for **2b** (51%) and **2c** (65%) due to material loss during the purification process, *i.e.*, due to the high sensitivity against oxygen and moisture and the high solubility of these complexes in nonpolar solvents like pentane or hexane.

The products obtained were in general sensitive towards air and moisture and not stable in many common solvents such as MeCN or chlorinated hydrocarbons, except for the cAAC-derivative **2a**, which proved to be more stable. The complexes **2a–g** were characterized by using elemental analysis, high resolution mass spectrometry (HRMS), NMR, IR and UV/VIS/NIR spectroscopy. However, low solubility and instability even in THF solutions of the complexes [Ni(I^{i}Pr)$_2$(I^{i}Pr-CS$_2$)] (**2f**) and [Ni(I^{i}Pr)$_2$(I^{i}Pr^{Me}-CS$_2$)] (**2g**) prevented characterization of these compounds in solution. HRMS measurements of highly diluted THF solutions of these compounds led to the detection of protonated molecular ions [M–H]$^+$. Nevertheless, CP/MAS (CP: cross polarization; MAS: magic angle spinning) NMR spectroscopic data obtained from solid samples of **2f–g** are in line with solution NMR data of **2a–e** and confirm the formation of the complexes [Ni(I^{i}Pr)$_2$(NHC-CS$_2$)] (NHC = I^{i}Pr and I^{i}Pr^{Me}, see below). The molecular structures of **2a–d** were confirmed by using single crystal X-ray diffraction (SC-XRD) analysis performed on single crystals obtained either from saturated toluene or from saturated THF solutions.

Solution NMR spectroscopy of complexes **2a–e** confirmed the presence of two I^{i}Pr NHC ligands coordinated to nickel, showing resonances in the ^{1}H and ^{13}C{^{1}H} NMR spectra of the complexes which were clearly shifted relative to the non-ligated I^{i}Pr. These I^{i}Pr shifts were in principle independent of the nature of the carbene-CS$_2$ co-ligand attached to nickel. Characteristic C*H*$_{methine}$ proton resonances were found in a small range of 6.05–6.27 ppm and the nickel-coordinated carbene carbon atom resonances were detected in a range between 181.2 ppm and 183.9 ppm. For complex **2a**, the signals of I^{i}Pr were split into two slightly shifted sets of resonances due to the asymmetry imposed by the coordinated cAAC^{Me}-CS$_2$ (**1a**) ligand. The coordinated azolium-2-dithiocarboxylate ligands in complexes **2** should be considered as dianionic 1,1-dithiolates (see Scheme 2) coordinated to Ni(II). This dianionic nature of the [carbene-CS$_2$]$^{2-}$ ligands in **2** is evident from the ^{1}H and ^{13}C {^{1}H} NMR spectroscopic shifts in solution as well as in the solid state (^{13}C and ^{15}N CP/MAS), which are significantly different from those of the non-coordinated, neutral carbene-CS$_2$ molecules. The most significant changes upon coordination were observed in the ^{13}C NMR resonances of the carbenoid (C=CS$_2$) and the CS$_2$ carbon atoms. While these resonances were found for the neutral carbene-CS$_2$ adducts **1a–g** at values in the range of 146.7–187.5 ppm (carbenoid, C1) and 219.7–229.2 ppm (CS$_2$, C2),[14b,h,14i,16,17] reductive coordination of the ligand led to shifts down to 130.0–141.5 ppm for the C1 carbon atom of the NHC and to 78.5–113.4 ppm for the C2 carbon atom of the CS$_2$ group. Moreover, these values differ clearly from values obtained for analogous 1,1-ene-dithiolate nickel complexes of the type [NiL$_2$(S$_2$C=CR$_2$)] (R = ketyl) bearing electronegative ketyl groups at the C2 carbon atom, which typically give rise to resonances at *ca.* 120 ppm (R$_2$C=CS$_2$, C1) and 210 ppm (CS$_2$, C2).[21] ^{13}C NMR values for comparable carbene-ligated CE$_2$ dianions (E = O, S) have so far not been reported.[17,22] Furthermore, in the ^{15}N CP/MAS NMR spectra of **2f–g**, two almost identically shifted low field resonances were detected at −173.5 ppm and −175.2 ppm for **2f** and at −173.3 ppm and −175.4 ppm for **2g**, which must be assigned to the nitrogen atoms of the NHC

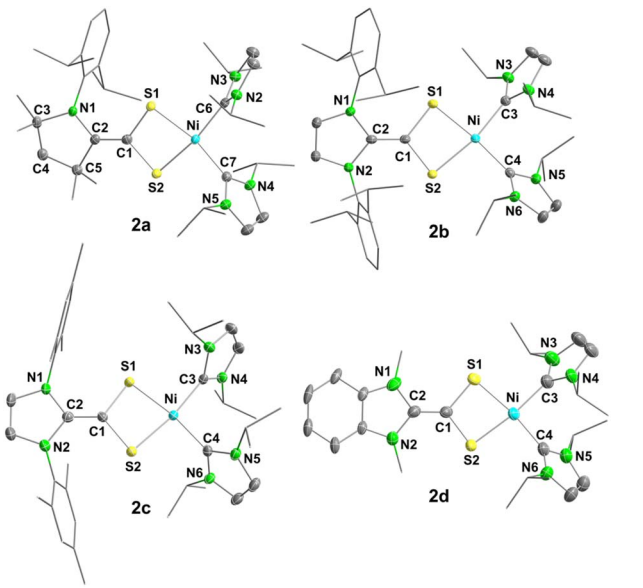

Fig. 1 Molecular structures of [Ni(I^{i}Pr)$_2$(cAAC^{Me}-CS$_2$)] (**2a**, top left), [Ni(I^{i}Pr)$_2$(IDipp-CS$_2$)] (**2b**, top right), [Ni(I^{i}Pr)$_2$(IMes-CS$_2$)] (**2c**, bottom left), and [Ni(I^{i}Pr)$_2$(BIMe-CS$_2$)] (**2d**, bottom right) in the solid-state (ellipsoids set at the 50% probability level). The hydrogen atoms were omitted for clarity. Selected bond lengths [Å] and angles [°] are provided within Table 1 or in the captions of Fig. S72–S75 of the ESI.‡

Table 1 Selected structural parameters of the complexes characterized by SC-XRD and related literature-known compounds. Bond lengths in Å and angles in °

	d(C–C)[a]	d(C–N)[b]	d(C–S)	d(S–M)	∡ SCS	∡ SMS[g]	∡ LML[e]	Twist-angle (∡ NCCS)[c]
[Ni(I^{i}Pr)$_2$(cAAC^{Me}-CS$_2$)] (**2a**)	1.343(2)	1.415(2)	1.776(1), 1.775(1)	2.188(1), 2.186(1)	102.7(1)	78.7(1)	101.3(1)	3.5(2)
[Ni(I^{i}Pr)$_2$(IDipp-CS$_2$)] (**2b**)	1.343(2)	1.417(2), 1.422(2)	1.768(1), 1.777(1)	2.179(1), 2.199(1)	103.8(1)	79.2(1)	96.3(1)	0.6(2), 5.4(2)
[Ni(I^{i}Pr)$_2$(IMes-CS$_2$)] (**2c**)	1.336(4)	1.421(3), 1.418(3)	1.776(3), 1.769(3)	2.180(1), 2.192(1)	103.6(1)	79.1(1)	97.4(1)	1.6(4), 0.4(4)
[Ni(I^{i}Pr)$_2$(BIMe-CS$_2$)] (**2d**)	1.341(3)	1.421(3), 1.417(3)	1.780(2), 1.769(2)	2.198(6), 2.185(1)	103.3(1)	78.8(1)	93.9(1)	8.2(4), 9.8(4)
[Ni(cAAC^{Me}-CS$_2$)$_2$] (**3a**)	1.391(2)	1.361(2)	1.740(1), 1.732(1)	2.190(1), 2.161(1)	105.4(1)	78.8(1)	—	5.9(2)
[Ni(IDipp-CS$_2$)$_2$] (**3b**)	1.395(2)	1.380(2), 1.378(2)	1.732(1), 1.730(1)	2.177(1), 2.181(1)	107.3(1)	79.6(1)	—	4.7(2), 3.6(2)
[Ni(IMes-CS$_2$)$_2$] (**3c**)	1.399(2)	1.377(2), 1.379(2)	1.734(1), 1.734(1)	2.174(1), 2.181(1)	106.8(1)	79.5(1)	—	6.5(2), 8.7(2)
K[Ni(cAAC^{Me}-CS$_2$)$_2$] (**4a^K**)	1.360(3), 1.353(3)	1.396(2), 1.399(2)	1.749(2), 1.763(2), 1.759(2), 1.763(2)	2.163(1), 2.187(1), 2.170(1), 2.180(1); 3.459(1),[g] 3.163(6)[g]	104.7(1), 104.2(1)	79.4(2), 79.5(1)	—	5.1(3), 3.9(3)
K[Ni(IDipp-CS$_2$)$_2$] (**4b^K**)	1.362(5), 1.378(5)	1.402(4), 1.401(4), 1.389(4), 1.389(4)	1.751(3), 1.766(3), 1.746(3), 1.757(3)	2.178(1), 2.184(1), 2.180(1), 2.199(1); 3.221(1),[g] 3.242(1)[g]	104.8(2), 105.8(2)	79.4(3), 79.3(3)	—	10.3(5), 11.9(5), 10.1(5), 13.4(5)
IMes-CS$_2$ (**1c**)[14h]	1.501(7)	1.315(4)	1.662(2)	—[f]	130.3(3)	—	—	87.5(3)
[Pd(PPh$_3$)$_2$(IMes-CS$_2$)]$^{2+15h}$	1.452(3)	1.351(3), 1.352(3)	1.692(2), 1.683(2)	2.334(1), 2.372(1)	113.5(1)	73.7(1)	101.1(1)	10.8(3), 12.0(3)
[K(18-crown-6)(IMes-CS$_2$)][16]	1.407(5)	1.388(4), 1.387(4)	1.734(3), 1.733(3)	3.216(1), 3.212(8)	124.0(2)	56.9(1)	—	31.2(4), 31.8(4)
[I^{i}Pr^{Me}-CS$_2$]$^{2-17}$	1.375(13)	1.455(10), 1.454(15)	1.803(8), 1.764(11)	3.156[d,h]	117.6(5)	—[f,h]	—	4.8(14), 8.4(14)

[a] Bond between the CS$_2$ group and the NHC carbene atom. [b] Bond to the NHC carbene carbon atom. [c] Dihedral angle. [d] Average value. [e] Considering the phosphorus or carbon atoms of the L-type ligands. [f] As the carbene-CS$_2$ moiety is not coordinated in a κ^2-*S*,*S*′ mode, no value is provided here. [g] Considering the sulfur atoms of the same ligand. [h] M = K.

ligands coordinated to nickel, as the nitrogen atoms of the dianionic ligands [I^{i}Pr-CS$_2$]$^{2-}$ and [I^{i}Pr^{Me}-CS$_2$]$^{2-}$ in **2f** and **2g** give rise to resonances at significantly more negative chemical shifts of −267.0 ppm in **2f** and −268.6 ppm in **2g**. This is in the typical signal range observed for delocalized enamines, in line with the formal Lewis structure of the dianionic redox state **C** (Scheme 2).[23] The nitrogen atoms of the NHC ligands attached to nickel most probably emerge as split resonances due to rotational freezing in the solid state.

In accordance with the spectroscopic data, the molecular structures of **2a–d** clearly indicated that these complexes are best described as bis-NHC nickel(II) complexes coordinated by the reduced dianionic [carbene-CS$_2$]$^{2-}$ ligands in a κ^2-*S*,*S*′ mode (Fig. 1 and Table 1).

The complexes **2a–d** adopt a distorted square planar geometry with bond angles ∡ CNiC between the carbene carbon atoms at the central nickel atom ranging between 93.9(1)° and 102.7(1)° and ∡ SNiS between the sulfur atoms of the azolium-2-dithiocarboxylate ligands at nickel in a narrow range of 78.8(1)° to 79.2(1)°. The carbene-CS$_2$ ligands undergo a series of structural changes upon coordination and internal reduction, *i.e.* electron transfer from the nickel atom to the ligand. The bond parameters indicate the presence of [carbene-CS$_2$]$^{2-}$ dianions (Scheme 2, form **C**) coordinated to the Ni(II) centers. For instance, the central dihedral angle ∡ NCCS (twist-angle) in **2a–d** ranges from 0.4(4)−9.8(4)°, indicating that the CS$_2$ group is almost ideally aligned co-planar to the NHC carbene plane, as reported previously for the dianion [I^{i}Pr^{Me}-CS$_2$]$^{2-}$ (∡ NCCS^{avg} = 6.6°).[17] In neutral azolium-2-dithiocarboxylates, these moieties are perpendicular to each other, and the radical monoanions such as [K(18-crown-6)(IMes-CS$_2$)] typically adopt twisted angles in-between ("twisted co-planar conformation"; for the potassium salt with ∡ NCCS^{avg} = 31.5°).[16] The reduction of the ligand system is accompanied by strengthening of the central C–C and weakening of the C–S and C–N bonds of the azolium-2-dithiocarboxylate ligands. This effect has also been observed for the one electron reduction as realized in [K(18-crown-6)(IMes-CS$_2$)],[16] and is expected to be even more pronounced in the complexes **2a–d**. The resulting bond lengths of **2a–d** are d(C–C) = 1.336(4)–1.343(2) Å, d(C–S) = 1.780(2)–1.768(1) Å and d(C–N) = 1.415(2)–1.422(2) Å, which are in line with the presence of C=C double bonds as well as C–N and C–S single bonds.[24] DFT geometry optimization of the complexes [Ni(I^{i}Pr)$_2$(cAAC^{Me}-CS$_2$)] (**2a**), [Ni(I^{i}Pr)$_2$(IDipp-CS$_2$)] (**2b**), [Ni(I^{i}Pr)$_2$(IMes-CS$_2$)] (**2c**), and [Ni(I^{i}Pr)$_2$(I^{i}Pr-CS$_2$)] (**2f**) at the PBE0-D3(BJ)/def2-TZVP(Ni)/def2-SVP(C,H,N,S) level of theory resulted in minimum structures with C=C distances of 1.352 Å (**2a**), 1.356 Å (**2b**), 1.355 Å (**2c**), and 1.365 Å (**2f**). In each case the HOMO is the C=C π-bonding orbital (see Fig. 2 and also Fig. S2 of the ESI‡), which confirms the presence of the dianionic ligand redox state **C**.[16] The differences in the geometrical data between coordinated and not coordinated ligands are also corroborated by calculated Wiberg bond indices (WBIs) obtained from the DFT-optimized (PBE0-D3BJ//def2-TZVP(Ni)/def2-SVP(C,H,N,S)) complexes [Ni(I^{i}Pr)$_2$(cAAC^{Me}-CS$_2$)] (**2a**), [Ni(I^{i}Pr)$_2$(IDipp-CS$_2$)] (**2b**), [Ni(I^{i}Pr)$_2$(IMes-CS$_2$)] (**2c**), and [Ni(I^{i}Pr)$_2$(I^{i}Pr-CS$_2$)] (**2f**) as well as the ligands cAAC^{Me}-CS$_2$ (**1a**),

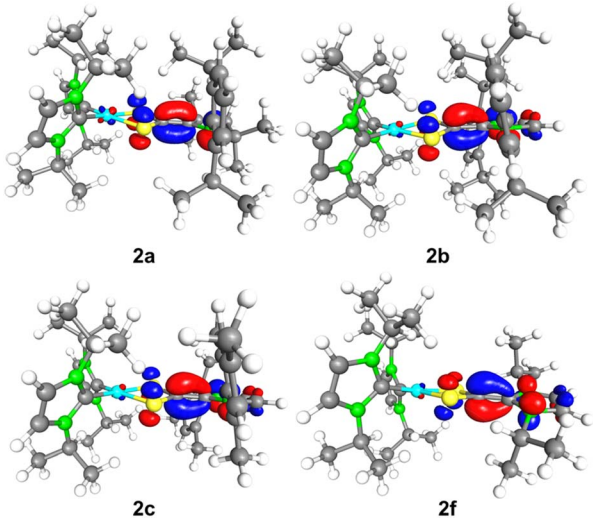

Fig. 2 Highest occupied molecular orbitals (HOMOs) of [Ni(I^{i}Pr)$_2$(-cAAC^{Me}-CS$_2$)] (**2a**, top left), [Ni(I^{i}Pr)$_2$(IDipp-CS$_2$)] (**2b**, top right), [Ni(I^{i}Pr)$_2$(IMes-CS$_2$)] (**2c**, bottom left) and [Ni(I^{i}Pr)$_2$(I^{i}Pr-CS$_2$)] (**2f**, bottom right) calculated at the PBE0-D3(BJ)/def2-TZVPP(Ni)/def2-TZVP(C,H,N,S) level of theory.

IDipp-CS$_2$ (**1b**), and IMes-CS$_2$ (**1c**). The WBIs for the C$_{carbene}$–C$_{CS2}$ bonds in **2a** (1.83), **2b** (1.73), **2c** (1.76), and **2f** (1.73) are much larger than those calculated for the pure ligands **1a–c** (0.95) and are consistent with double bond character (see Table S3 of the ESI‡). Accordingly, the WBIs for the C–N and C–S bonds decrease upon coordination from 1.25–1.44 (C–N) for **1a–c** to 1.02–1.07 for **2a–f** and from 1.48/1.49 (C–S) for **1a–c** to 1.00–1.03 for **2a–f**, respectively. All these factors are consistent with the transfer of two negative charges to the ligand.

Reductive ligation of azolium-2-dithiocarboxylates also leads, in general, to a decrease in the bite angle ∡SCS relative to the neutral free ligands (*e.g.* IMes-CS$_2$: ∡SCS = 130.3(3)°), which results in ∡SCS angles in a range of 102.7(1)–103.8(1)° for complexes **2a–d**. Interestingly, the bonding parameters observed for the azolium-2-dithiocarboxylate ligands in **2a–d** differ significantly from those reported for the related square planar dicationic complex [Pd(PPh$_3$)$_2$(κ^2-*S*,*S*′-IMes-CS$_2$)]$^{2+}$[15h] with (average) bond lengths of C–C: 1.452 Å, C–N: 1.352 Å and C–S: 1.688 Å, which closely resemble those of the neutral non-ligated IMes-CS$_2$ molecule (d(C–C) = 1.452(3) Å, d^{avg}(C–N) = 1.315(4) Å; d^{avg}(C–S) = 1.662(2) Å).[14h] This deviation can be attributed to the difference in the total charge of both complexes (0 *vs.* +II), which does not affect the oxidation state of the central metal atoms (Ni(II) *vs.* Pd(II)) but influences the redox state of the IMes-CS$_2$ ligand, which is dianionic in **2a–d** and neutral in [Pd(PPh$_3$)$_2$(κ^2-*S*,*S*′-IMes-CS$_2$)]$^{2+}$.

As the ligation of azolium-2-dithiocarboxylates with nickel(0) complexes bearing two additional NHC ligands (I^{i}Pr) led to the internal reduction of the carbene-CS$_2$ ligands forming 1,1-dithiolate complexes of nickel(II), we were interested in investigating how two of such ligands would behave in homoleptic nickel complexes in the absence of additional co-ligands. Therefore we reacted [Ni(COD)$_2$] (COD = 1,5-cyclooctadiene) with the CS$_2$ adducts of the *N*-aryl substituted carbenes cAAC^{Me}-CS$_2$ (**1a**), IDipp-CS$_2$ (**1b**) and IMes-CS$_2$ (**1c**). Solutions (**1a**) or suspensions (**1b–c**) of azolium-2-dithiocarboxylates in toluene react cleanly with [Ni(COD)$_2$] at room temperature, leading to immediate dissolution and a color change in the reaction mixtures from yellow to green-purple (**3a**) or to blue and then dark-green (**3b–c**). The homoleptic bis-azolium-2-dithiocarboxylate complexes [Ni(cAAC^{Me}-CS$_2$)$_2$] (**3a**), [Ni(IDipp-CS$_2$)$_2$] (**3b**) and [Ni(IMes-CS$_2$)$_2$] (**3c**) were isolated as microcrystalline powders in yields of 78–80% after workup (Scheme 5).

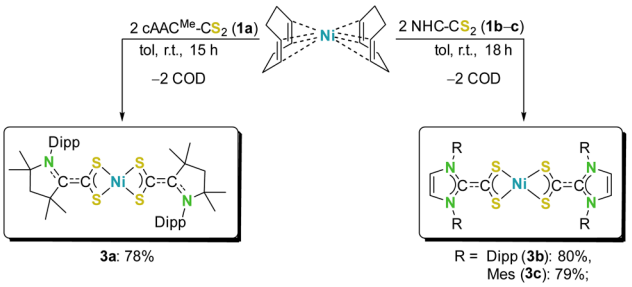

Scheme 5 Synthesis of homoleptic bis-azolium-2-dithiocarboxylate nickel complexes **3a–c**.

Compounds **3a–c** were characterized using elemental analysis, HRMS, NMR, IR and UV/VIS/NIR spectroscopy, as well as cyclic voltammetry (CV) and SC-XRD analysis using single crystals obtained from saturated benzene or THF solutions. The homoleptic bis-(carbene-CS$_2$) complexes **3a–c** in general were less sensitive towards air or moisture than their heteroleptic relatives **2a–g**, with **3a** being the most stable complex.

NMR spectroscopy of solutions of the complexes **3a–c** revealed characteristic sets of signals of the carbene scaffolds in the ^{1}H NMR spectra, which were shifted relative to the resonances of the free ligands **1a–c** to values characteristic for diamagnetic compounds. Interestingly, the ^{13}C{^{1}H} NMR spectra recorded for **3a–c** did not show resonances for the carbenoid carbon atom and the CS$_2$ carbon atoms of the carbene-CS$_2$ ligands, whereas all the peripheral carbon resonances were detected in the range expected (see Fig. S27, S29, S31 of the ESI‡). We attribute this behavior to considerable electronic mixing of an energetically low-lying triplet state into the singlet ground state of the molecule (see below).

The complexes **3a–c** crystallize in the space groups $P\bar{1}$, $P2_1/n$ and $P2_1/c$. The results of the X-ray analyses reveal that these complexes are homoleptic coordinated bis-azolium-2-dithiocarboxylate complexes of Ni(II) in a distorted square planar environment (Fig. 3 and Table 1). Both azolium-2-dithiocarboxylates are attached *via* two κ^2-*S*,*S*′ interactions to nickel and the molecular units crystallize without considerable intermolecular interactions between the molecular entities of **3a–c** (compare Fig. S77, S78, S80, S81, S83 and S84‡ for unit cell packing), which is most probably hindered by the steric bulk of the *N*-aryl groups of **3a–c**. Thus, the intermolecular distances from the nickel atom of one molecular entity to the NiS$_4$ plane of the next parallelly aligned molecular unit are 6.258(1) Å (**3a**), 10.473(1) Å (**3b**) and 6.680(1) Å (**3c**).

Similar to **2a–d**, the redox state of the carbene-CS$_2$ ligands in **3a–c** is altered upon coordination to nickel, leading to internal

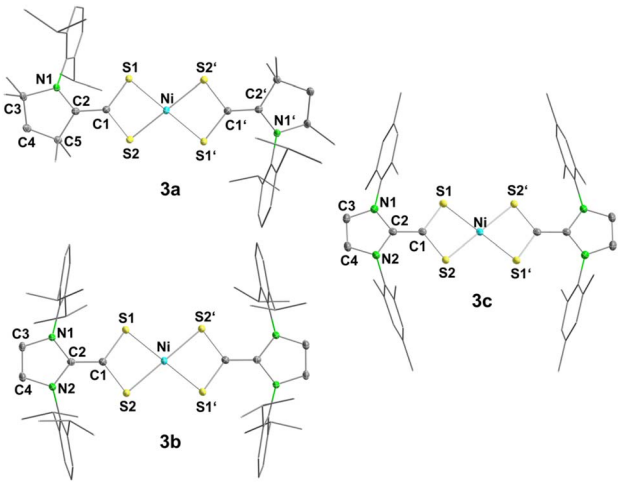

Fig. 3 Molecular structures of [Ni(cAAC^{Me}-CS_2)$_2$] (**3a**, top left), [Ni(I-Dipp-CS_2)$_2$] (**3b**, bottom left) and [Ni(IMes-CS_2)$_2$] (**3c**, middle right) in the solid-state (ellipsoids set at the 50% probability level). The hydrogen atoms and co-crystallized solvent molecules are omitted for clarity. Selected bond lengths [Å] and angles [°] are provided within Table 1 or in the captions of Fig. S76, S79 and S82 of the ESI.‡

reduction and structural changes within the ligand system. In **3a–c**, the present oxidation state of the central nickel ions may therefore be deduced by considering the changes in the bond parameters of the attached carbene-CS_2 ligands, which indicate the presence of d^8-nickel(II) ions, which is also in line with the adoption of a square planar geometry. These nickel(II) ions are coordinated by two radical monoanionic [carbene-CS_2]$^{\bullet-}$ ligands (redox state **B**, Scheme 2) as a result of internal reduction (for a theoretical assessment, see below). This is corroborated by C–C bond strengthening, as well as C–N and C–S bond weakening compared to the non-coordinated azolium-2-dithiocarboxylates. This happens to a degree similar to that observed for the radical monoanions of the type [K(18-crown-6)(carbene-CS_2)] reported recently,[16] but is less pronounced than that observed for the complexes **2a–d** presented above. The bond lengths observed for **3** range in between 1.391(2) Å and 1.399(2) Å (C–C), 1.361(2) Å and 1.380(2) Å (C–N) as well as 1.730(1) Å and 1.740(1) Å (C–S). The [carbene-CS_2]$^{\bullet-}$ ligands adopt almost ideal co-planar conformations with dihedral angles ∡NCCS in the range of 3.6(2)–8.7(2)°. Thus, co-planarity extends across both radical anionic 1,1-dithiolate ligands and the central nickel atom. Furthermore, the bite angles ∡SCS of 105.4(1)–107.3(1)° observed are slightly smaller than those observed in complexes **2a–d**, where the carbene-CS_2 ligands carry a dianionic charge. These metric data are also corroborated by the calculated WBIs obtained from DFT-optimized (PBE0-D3BJ//def2-TZVP(Ni)/def2-SVP(C,H,N,S)) complexes [Ni(cAAC^{Me}-CS_2)$_2$] (**3a**), [Ni(IDipp-CS_2)$_2$] (**3b**) and [Ni(IMes-CS_2)$_2$] (**3c**). The WBIs for the $C_{carbene}$–C_{CS2} bonds of 1.45 (**3a**), 1.40 (**3b**), and 1.44 (**3c**) lie between those calculated for the pure ligands **1a–c** (0.95) and the NHC-ligated complexes [Ni(I^{i}Pr)$_2$(carbene-CS_2)] **2a–c**, **2f** (1.73–1.83); similarly the WBIs for the C–N and C–S bonds align with this trend (see Table S3 of the ESI‡), which is consistent with the transfer of one negative charges to each ligand.

DFT calculations have been performed at different levels of theory to elucidate the electronic structure of the bis-(carbene-CS_2)-ligated nickel complexes **3**. A molecular orbital diagram of the frontier orbitals of D_{2h}-symmetric [Ni(IMes-CS_2)$_2$] (**3c**), calculated at the B3-LYP//def2-TZVP(Ni)/def2-SVP(C,H,N,S) level of theory, is provided in Fig. 4 and S3 of the ESI.‡

Within the D_{2h}-symmetry restraint, the orbitals in the region between −4.3 eV and −6.5 eV are either located on the sulfur atoms and can be described as lone pairs on sulfur or are the typical metal d-centered orbitals of a square planar complex. The unoccupied orbital $33b_{2g}$ at −0.63 eV is the σ*-antibonding Ni-centered $x^2 - y^2$ orbital of the square plane. The electronic structure of D_{2h}-[Ni(IMes-CS_2)$_2$] is dominated by the $20b_{2u}$ orbital at −3.09 eV, which is the HOMO of the complex and the $19b_{1g}$ orbital at −2.09 eV, which corresponds to the LUMO. Both orbitals are in principle linear combinations of the $C_{carbene}$=□ C_{CS2} π-orbitals mentioned earlier. The occupied orbital $20b_{1u}$ (denoted as π_1 in Fig. 4) is the symmetric linear combination with both π-bonds in phase, whereas the unoccupied orbital $19b_{1g}$ (denoted as π_2 in Fig. 4) is the asymmetric linear combination of these π-bonds with some antibonding admixture of a metal 3d orbital. The gap between both orbitals is merely 1.00 eV. Due to this small HOMO/LUMO gap a triplet state is relevant for **3c**, which lies only 11.6 kJ mol^{-1} above the

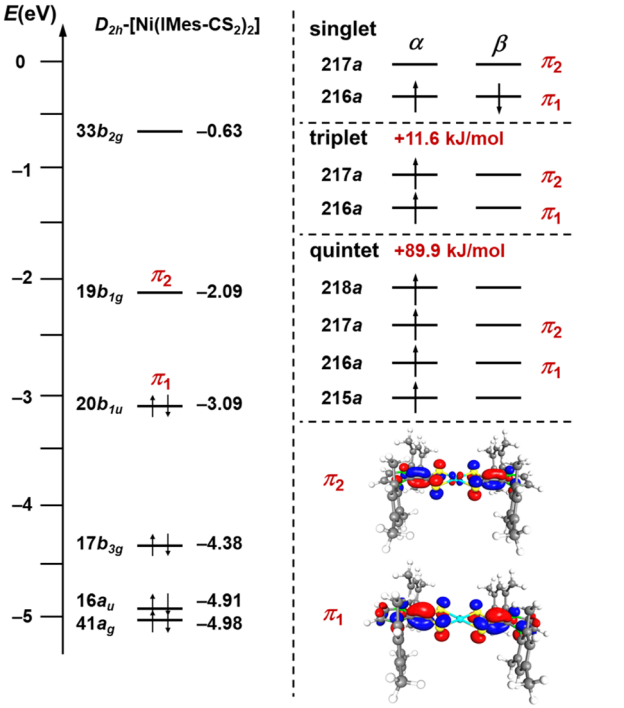

Fig. 4 Molecular orbital diagram obtained from DFT calculations on geometry-optimized, D_{2h}-symmetric [Ni(IMes-CS_2)$_2$] (**3c**) at the B3-LYP//def2-TZVP(Ni)/def2-SVP(C,H,N,S) level of theory and the relative energies of the singlet, triplet, and quintet state of this complex. The MOs and an overview of the changes in selected geometric parameters of **3c** in different electronic states are provided in Fig. S3 and S4 of the ESI.‡

singlet ground state, where the orbitals π_1 and π_2 are singly occupied by electrons of the same spin. In addition to the triplet state, a quintet state, where one electron of the $17b_{3g}$ orbital is formally promoted to MO $33b_{2g}$, lies 89.9 kJ mol^{-1} above the singlet diradical state.

If the symmetry constraints are removed, the HOMO $20b_{1u}$ becomes MO 216*a* and the LUMO $19b_{1g}$ becomes MO 217*a*, and the ground state of this molecule can be described as a singlet diradical, which is in accordance with the electronic structure of closely related palladium complexes reported recently.[15s] However, significant mixing of the singlet and the triplet state occurs, which stabilizes the molecule. Geometry optimizations of [Ni(IMes-CS_2)$_2$] (**3c**) for the closed shell and open shell complexes at different levels of theory (functional B3-LYP and PBE0-D3BJ; basis sets def2-TZVP(Ni)/def2-SVP(C,H,N,S) and def2-TZVPP(Ni)/def2-TZVP(C,H,N,S)) reveal that the unrestricted open shell singlet diradical ground state is energetically favored compared to the restricted closed shell state, but it is heavily spin-contaminated (S^2 statistics of 0.752–0.867 for **3c**, depending of the level of theory, for details see Tables S1 and S2 of the ESI‡). For example, the open shell singlet diradical is favored by 21.2 kJ mol^{-1} compared to the closed shell singlet at the B3-LYP//def2-TZVP(Ni)/def2-SVP(C,H,N,S) level. If spin-contamination of the singlet diradical state originates exclusively from the mixing of the low-lying triplet state into the singlet diradical state an S^2 value of 0.80 would account for roughly 40% admixture of the triplet into the singlet state. Geometry optimization of the closed shell singlet, open shell singlet, triplet, and quintet state leads to slight changes in the geometries of **3c** (see Fig. S4 of the ESI‡). Especially the Ni–S distances widen upon going from the closed shell singlet (2.2201 Å) to the triplet state (2.2607 Å), and the calculated bond lengths for the open shell singlet diradical lie in-between (2.2477 Å).

The same features as described in detail for [Ni(IMes-CS_2)$_2$] (**3c**) also apply to the complexes [Ni(cAAC^{Me}-CS_2)$_2$] (**3a**) and [Ni(IDipp-CS_2)$_2$] (**3b**), which show singlet diradical ground states with significant admixtures of energetically low-lying triplet states (see Tables S1 and S2 of the ESI‡). The spin orbitals of the π_1 orbital and the spin densities of the singlet diradical ground states of [Ni(cAAC^{Me}-CS_2)$_2$] (**3a**), [Ni(IDipp-CS_2)$_2$] (**3b**), and [Ni(IMes-CS_2)$_2$] (**3c**), calculated at the B3-LYP//def2-TZVP(Ni)/def2-SVP(C,H,N,S) level, are presented in Fig. 5 (**3c**) and S5 (**3a** and **3b**, see ESI).‡

In each of the congeners **3a–c** the orbital π_1 is the HOMO of the complex and each spin orbital $\pi_1(\alpha)$ and $\pi_1(\beta)$ is centered on a different dithiolato ligand. Thus, the spin density plot of each complex clearly reveals that the spin densities for up and down spins are located on different dithiolato ligands. The open-shell singlet ground state therefore demonstrates that SOMO1 and SOMO2 (SOMO = singly occupied molecular orbital) are localized on different ligands, which agrees with a description of the azolium-2-dithiocarboxylates in **3a–c** as radical monoanionic ligands and a nickel atom in the oxidation state +II.

The nickel complexes ligated with the anionic carbene-CS_2 ligands reported herein should, in principle, exhibit distinctly different C–C vibrations in comparison to the neutral ligands due to C–C bond strengthening upon reductive complexation. However, DFT calculations at the B3-LYP//def2TZVP(Ni)/def2SVP(C,H,N,S) level of theory predicted for **3b** several vibrations at 1353 cm^{-1} (asymmetric stretching vibration + CN coupling), 1323 cm^{-1} (symmetric stretching vibration + CN coupling), 1259 cm^{-1} and 1243 cm^{-1} (C–N stretches C–C coupling), which showed significant coupling of the C–C stretches with the vibrations of the imidazolium ligand frame. As the relevant range in the experimental IR spectra were additionally overlayed with other vibrations of similar intensities, the C–C stretches of these complexes were not unambiguously allocated and are thus not discussed herein.

Time-dependent (TD) DFT calculations at the PBE0-D3BJ//def2-TZVPP(Ni)/def2-TZVP(C,H,N,S)/COSMO(benzene) level using the singlet ground state of the complexes predicted characteristic intense absorptions of the complexes **3a–c** in the near-IR region at 1008 nm (**3a**), 1034 nm (**3b**) and 1056 nm (**3c**) (Fig. S6 of the ESI‡), which were assigned as ligand-to-ligand charge transfer (LLCT) transitions from the π_1 to the π_2 orbital. This was also confirmed by experimental UV/VIS/NIR spectroscopic measurements of complexes **3a–c** in benzene (see Fig. 6).

The UV/VIS/NIR spectra of all three compounds **3a–c** reveal the same absorption pattern with similar values of λ_{abs} featuring two intense absorptions in the ultra-violet region (*ca.*: 292 nm and 367 nm), two less-intense, broad absorptions in the visible region (*ca.*: 462 nm and 711 nm) and an intense absorption in the NIR region (ω_1) at almost identical values of 1076 nm (**3a**), 1077 nm (**3b**) and 1064 nm (**3c**), which is qualitatively in line with the predicted values obtained from TD-DFT calculations (see discussion above, λ_{calc} = 1008 nm (**3a**), 1034 nm (**3b**), and 1056 nm (**3c**)). These NIR absorptions ω_1 of the nickel complexes **3a–c** are absent in the complexes **2** with formally dianionic ligands [carbene-CS_2]$^{2-}$ (see Fig. S54–S56 of the ESI‡) and lie at almost the same energies as those observed for some palladium congeners reported previously, such as

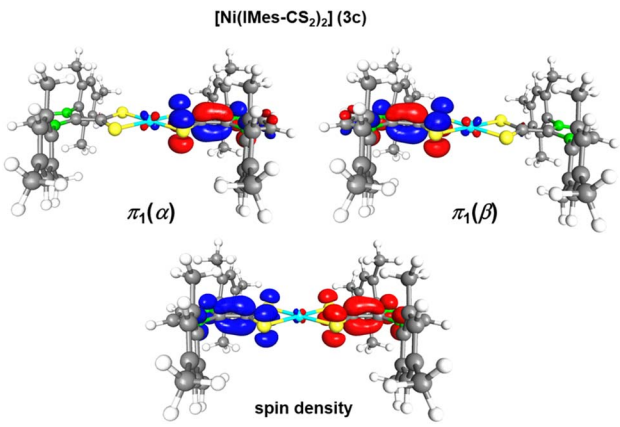

Fig. 5 π_1 spin orbitals $\pi_1(\alpha)$ (216*a*,α) and $\pi_1(\beta)$ (216*a*,β) and the spin densitiy (blue: spin up and red: spin down) of the singlet diradical ground states of [Ni(IMes-CS_2)$_2$] (**3c**) calculated at the B3-LYP//def2-TZVP(Ni)/def2-SVP(C,H,N,S) level of theory. The spin-densities calculated for **3a** and **3b** are provided in Fig. S5 of the ESI.‡

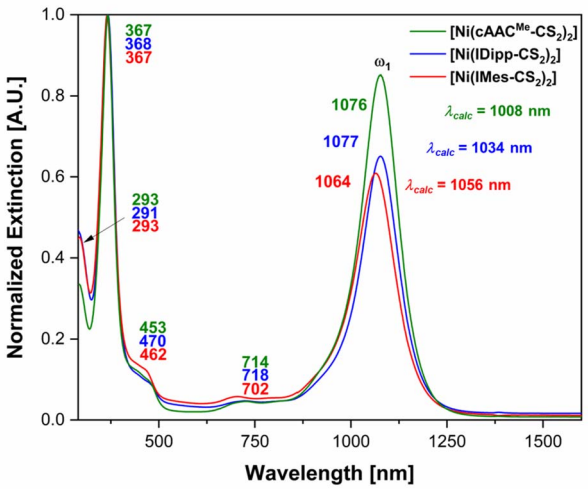

Fig. 6 Experimental UV/VIS/NIR spectra of [Ni(cAAC^{Me}-CS$_2$)$_2$] (**3a**, green), [Ni(IDipp-CS$_2$)$_2$] (**3b**, blue) and [Ni(IMes-CS$_2$)$_2$] (**3c**, red) in benzene and TD-DFT (PBE0-D3BJ//def2-TZVPP(Ni)/def2-TZVP(C,H,N,S)/COSMO(benzene)) calculated absorption maxima λ_{calc} for the NIR absorption (ω_1).

[Pd(IDipp-CS$_2$)$_2$],[15s] which absorbs at 1014 nm. This NIR absorption is an intrinsic feature of these neutral complexes [M(IDipp-CS$_2$)$_2$] and seems to be independent of substitutional variations in the system.

However, the choice of the central metal atom affects the redox-chemical properties in the systems [M(carbene-CS$_2$)$_2$], which are governed by (quasi)reversible one-electron processes corresponding to oxidation or reduction reactions addressing the π_1 or π_2 ligand centered orbitals. Cyclic voltammetric measurements performed on the complexes **3a–c** (Fig. 7; all

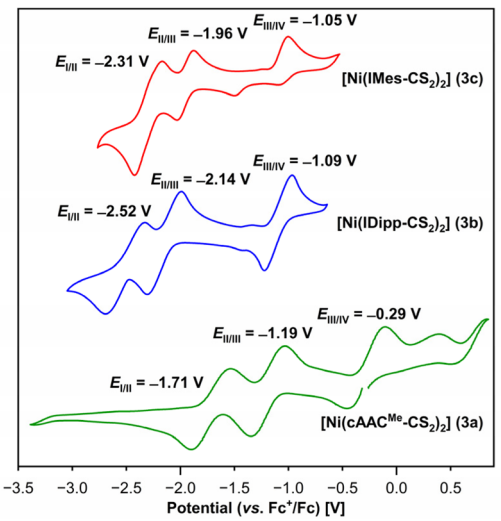

Fig. 7 Cyclic voltammograms of [Ni(cAAC^{Me}-CS$_2$)$_2$] (**3a**, green, bottom), [Ni(IDipp-CS$_2$)$_2$] (**3b**, blue, middle) and [Ni(IMes-CS$_2$)$_2$] (**3c**, red, top) in THF (concentrations *ca.* 1 mM) with added [TBA][PF$_6$] (TBA = tetra(*n*-butyl)ammonium; 0.1 M). Potentials are internally referenced relative to the ferrocenium/ferrocene (Fc$^+$/Fc) couple with negative sweep directions. Scan velocities $v = 25$ mV s^{-1} (**3a**, **3c**), 50 mV s^{-1} (**3b**).

potentials referenced *vs.* the ferrocenium/ferrocene (Fc$^+$/Fc) redox couple) in THF thus revealed two redox events ($E_{II/III}$, $E_{III/IV}$) corresponding to step-wise one-electron oxidations of the nickel(II)-ligated radical monoanions [carbene-CS$_2$]$^{\cdot-}$ to the respective neutral forms, which leads to mono- ($E_{II/III}$) and dicationic ($E_{III/IV}$) complexes [Ni(carbene-CS$_2$)]$^{+/2+}$ (**3a**: $E_{II/III} = -1.19$ V and $E_{III/IV} = -0.29$ V; **3b**: $E_{II/III} = -2.14$ V and $E_{III/IV} = -1.09$ V; **3c**: $E_{II/III} = -1.96$ V and $E_{III/IV} = -1.05$ V). While the oxidation step $E_{II/III}$ is reversible for all complexes **3a–c**, the second oxidation step to yield the dication $E_{III/IV}$ shows decreasing reversibility in the order **3b** < **3a** < **3c**. In comparison, the one-electron oxidation processes $E_{II/III}$ and $E_{III/IV}$ in **3a–c** occur at significantly more negative potentials than those observed for the palladium congeners. For example, for [Pd(I-Dipp-CS$_2$)$_2$], two reversible processes were reported at −0.97 V ($E_{II/III}$; *vs.* **2b**: −2.14 V) and −0.325 V ($E_{III/IV}$; *vs.* **2b**: −1.09 V) in total.[15s] Moreover, for the nickel complexes **3a–c** we observed an additional third reversible redox event in the cyclic voltammograms at even more negative potentials, which may be assigned to a one-electron reduction, yielding the corresponding nickelates [Ni(carbene-CS$_2$)$_2$]$^{\cdot-}$ (**3a**: $E_{I/II} = -1.71$ V; **3b**: $E_{I/II} = -2.52$ V; **3c**: $E_{I/II} = -2.31$ V), where the low-lying π_2 LUMO is involved. All three redox events $E_{I/II}$, $E_{II/III}$ and $E_{III/IV}$ in general occur at more positive potentials for the cAAC-based compound **3a**, *i.e.*, the formation of the nickelate anion, as well as the mono- and dications is easier to achieve for the cAAC derivative **3a**, which also reflects the better π-accepting properties of cAACs compared to NHCs.[19i,26]

In light of these results, the synthesis and isolation of monoanionic, radical nickelates of the type [Ni(carbene-CS$_2$)$_2$]$^{\cdot-}$ posed a challenge, which is achievable by reduction of the neutral nickel complexes **3a–c** with metallic reductants.

If solutions of **3a–c** in THF were treated with an excess of KC$_8$ or [CoCp$_2$] (for **3a**) at room temperature the reaction mixtures immediately changed their color from dark green to yellow-green (**3a**) or red (**3b–c**). Workup of the reaction mixtures led to isolation of salts of the radical monoanionic nickelates [Cat]$^+$[Ni(cAAC^{Me}-CS$_2$)$_2$]$^-$ (Cat = K: **4a^K**, CoCp$_2$: **4a^{Co}**) and K$^+$[Ni(IDipp-CS$_2$)$_2$]$^-$ (**4b^K**) in 70% (**4a^K**), 71% (**4a^{Co}**) and 41% (**4b^K**) yield (Scheme 6).

The isolated paramagnetic nickelate salts **4a–b** were characterized by EPR, IR and UV/VIS/NIR spectroscopy as well as SC-

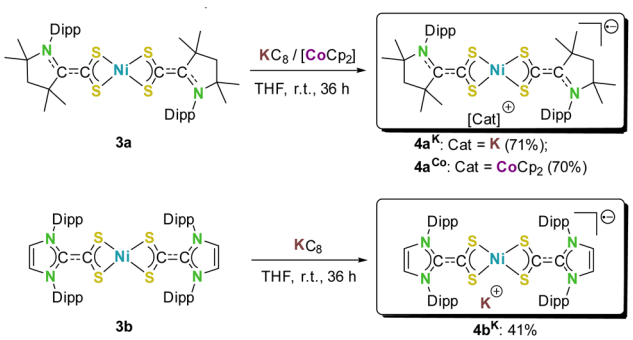

Scheme 6 Synthesis of the nickelates [Cat][Ni(carbene-CS$_2$)$_2$] (**4a–b$^{K/Co}$**; Cat = K, CoCp$_2$).

XRD, elemental analysis and HRMS. High resolution mass spectrometry of THF solutions of **4a–b^{K}** proved that the central [Ni(carbene-CS_2)$_2$] moiety remains intact upon reduction, as the [Ni(carbene-CS_2)$_2$]$^{\cdot-}$ molecular ion peaks (m/z = 780.3161 (**4a^{K}**) and 986.4016 (**4b^{K}**)) were detected. Instantaneous re-formation of the neutral complexes **3a–b** was observed upon exposure of the complexes to air, as indicated by the characteristic dark green (**3b**) or green-purple (**3a**) color of the neutral compounds and the corresponding NMR and UV/VIS/NIR spectra, which revealed the characteristic resonances or absorptions of **3a–b**.

Single crystals of **4a–b^{K}** were obtained from saturated THF solutions and used for SC-XRD analyses, which confirmed the molecular structures as the potassium salts of nickelate anions [Ni(carbene-CS_2)$_2$]$^{\cdot-}$ (Fig. 8 and Table 1).

The salts **4a^{K}** and **4b^{K}** crystallize in the space groups $P2_1/n$ and $P2_12_12_1$ and contain intact, non-stacked monoanionic square planar nickelates [Ni(carbene-CS_2)$_2$]$^{\cdot-}$. The potassium cations are attached to two of the sulfur atoms (d(S–K) = 3.163(6)–3.459(1) Å), with a separation from the central nickel atoms of d(Ni–K) = 3.615(1) Å and 3.358(1) Å). The potassium cations are coordinatively saturated by complexation of three THF ligands in **4a^{K}** or two THF ligands in **4b^{K}**. As observed in the molecular structures of the carbene-CS_2 compounds **2a–d** and **3a–c**, the difference in the ligands' redox states for the nickelates **4a–b^{K}** can be deduced from the change in bond parameters which can be attributed to ligand-centered reductions and occupation of the π_2 LUMOs of the neutral complexes (Fig. 4). In both nickelates **4a–b^{K}**, the two carbene-CS_2 ligands are found with almost identical bond lengths (d(C–C) = 1.353(3)–1.378(5) Å, d(C–N) = 1.389(4)–1.402(4) Å, and d(C–S) = 1.746(3)–1.766(3) Å), which are between those of the dianionic (**C**; *e.g.* **2a–d**) and the radical monoanionic (**B**; *e.g.* **3a–c**) ligand forms (see Table 1). This geometrical change is, again, also reflected in the Wiberg bond indices calculated for the DFT-optimized (PBE0-D3BJ//def2-TZVP(Ni)/def2-SVP(C,H,N,S)) nickelates [Ni(cAAC^{Me}-CS_2)$_2$]$^{\cdot-}$ (**4a**) and [Ni(IDipp-CS_2)$_2$]$^{\cdot-}$ (**4b**). The WBIs for the $C_{carbene}$–C_{CS2} bonds of 1.70 (**4a**) and 1.59 (**4b**) are higher than those calculated for the neutral complexes **3a** (1.45) and **3b** (1.40) and almost reach the values calculated for the related NHC-ligated complexes [Ni(I^{i}Pr)$_2$(carbene-CS_2)] **2a** (1.83) and **2b** (1.73). Similarly, the WBIs calculated for the C–N and C–S bonds of **4a** and **4b** reach values close to those calculated for **2a** and **2b** (see Table S3 of the ESI‡), which is consistent with the additional negative charge delocalized over both ligands.

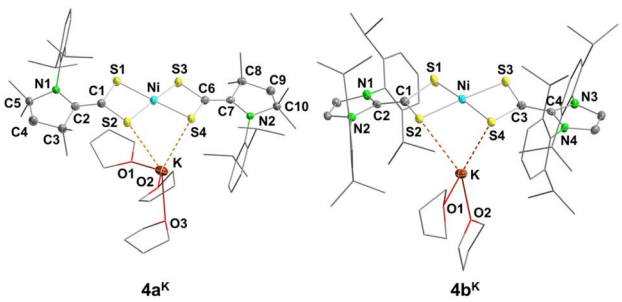

Fig. 8 Molecular structures of [K(THF)$_3$][Ni(cAAC^{Me}-CS_2)$_2$] (**4a^{K}**, left) and [K(THF)$_2$][Ni(IDipp-CS_2)$_2$] (**4b^{K}**, right) in the solid-state (ellipsoids set at the 50% probability level). The hydrogen atoms are omitted for clarity. Selected bond lengths [Å] and angles [°] are given in Table 1 or in the captions of Fig. S85 and S88.‡ The unit cell packing of these complexes are provided in Fig. S86–S90 of the ESI.‡

Reduction with coordination of the potassium cations comes along with a slight distortion of the overall square planar structure of the complexes. This distortion is visualized in Fig. S7 of the ESI,‡ which provides side-on perspectives of the experimentally obtained molecular structures of the neutral compounds **3a–b** *vs.* the anions **4a–b^{K}**. Thus, in **4a^{K}** and **4b^{K}**, the angles ∡SNiS between sulfur atoms in *trans* positions deviate from the ideal 180° angle as observed in the square planar neutral compounds **3a** and **3b**, with coordination to nickel at angles of 173.5(1)° or 178.2(1)° (**4a^{K}**) and 173.6(1)° or 177.0(1)° (**4b^{K}**). Furthermore, minor curving of the overall planar structures of **3a–b** is observed in **4a–b^{K}** with the ligand frames bending towards the attached potassium ions. The latter is reflected by an increase in the angles between the C–C vectors of the bonds between the CS_2 groups and the carbenoid carbon atoms with respect to the central NiS_4 square planes. Thus, in the nickelate **4b^{K}** the angles ∡(vector(CC)−plane(NiS4)) are 9.2(1)° and 13.8(1)° for both ligands, while for the neutral form **3b**, values of 3.7(1)° are found. In the cAAC derived nickelate **4a^{K}**, analogous bending of the ligand frame in one direction is found, although to a smaller degree as in **4b^{K}**, which is reflected by respective angles ∡(vector(CC)−plane(NiS_4)) of 1.7(1)° and 9.1(1)°. Contrastingly, in the neutral compound **3a**, both ligands are bent in opposite directions away from the central NiS_4 square plane by 7.3(1)°. Furthermore, the (average) twist angles ∡NCCS of the CS_2 group relative to the attached carbene increase to 11.4° for the nickelate **4b^{K}** relative to the neutral form **3b**, while in **4a^{K}** this twisting slightly decreases to 4.5° relative to neutral **3a** which has an angle of 5.9(2)°.

Quantum chemical geometry optimizations (see Fig. S8 of the ESI,‡ top) resulted in a similar distorted geometry for the free nickelate **4b** (calc.: ∡(vector(CC)–plane(NiS_4)) = 20.9°, 27.7°; ∡SNiS = 171.1°, 171.7°), while for **4a** an almost undistorted structure was obtained (calc.: ∡(vector(CC)–plane(NiS_4)) = 0.9°; ∡SNiS = 180°). We attribute the observed structural distortion of the nickelates **4a–b^{K}** to the additional electron, which is delocalized over both ligands and results in [carbene-CS_2]$^{1.5-}$ ligands, while the oxidation state of the nickel atom remains unchanged. DFT calculations (see Fig. S8 of the ESI,‡ bottom) confirm that the spin density of the nickelates **4a** and **4b** is delocalized over the whole molecule. Thus, due to the almost indistinguishable nature of both carbene-CS_2 ligands in **4a–b^{K}**, the metalla-anions should be considered as ligand based mixed-valent (LBMV) systems which feature strong electronic coupling between both ligands, similar to Robin-Day class III systems.[27]

The additional electron in the nickelates **4a–b^{K}** leads to paramagnetic character of the metallates, which was confirmed *via* X-band EPR spectroscopy (Fig. 9) performed on THF solutions of the complexes at 70 K. These EPR spectra revealed broad resonances without resolved hyperfine coupling (Fig. 9).

For both compounds **4a^{K}** and **4b^{K}**, rhombic g-tensors were found (**4a^{K}**: g_1 = 2.0357, g_2 = 2.0413, and g_3 = 2.1274; **4b^{K}**: g_1 =

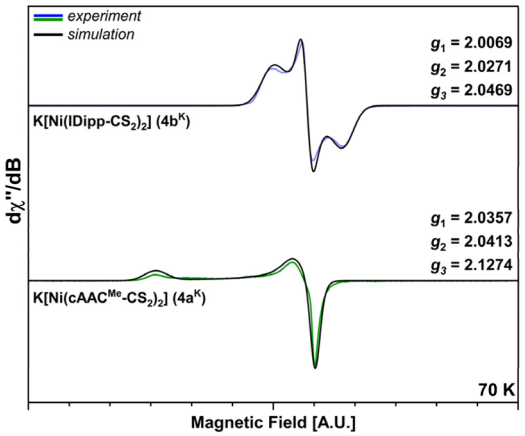

Fig. 9 βX-band EPR spectra of K[Ni(cAAC^{Me}-CS$_2$)$_2$] (**4a^K**, bottom, green) and K[Ni(IDipp-CS$_2$)$_2$] (**4b^K**, top, blue) at 70 K with normalized *x*- and *y*-axes (exact values are provided in Fig. S32–S34 of the ESI;‡ resonances are detected at *ca.* 310–340 mT; black lines: simulated spectra; regular, colored lines: experimental spectra).

2.0069, $g_2 = 2.0271$, and $g_3 = 2.0469$), both matching simulations. The obtained EPR data are essentially in line with spin systems of square planar symmetry[28] and other EPR-characterized nickel bis-dithiolene monoanions reported earlier.[25a] The significant differences in *g* anisotropy between **4a^K** and **4b^K** can be attributed to the different degrees of structural distortion observed in the anions, as well as to different spin distributions of the anions (see Fig. S8 of the ESI,‡ bottom), with **4a^K** exhibiting a more localized unpaired spin, while **4b^K** features a highly delocalized spin across both ligand moieties.

UV/VIS/NIR spectroscopy on THF solutions of the nickelate compounds **4a^K** and **4b^K** were performed to evaluate the absorption properties of the bis-(carbene-CS$_2$) complexes **3** upon reduction (Fig. 10). Intriguingly, while the neutral complexes **3a–c** absorb at *ca.* 1076 nm, in the respective anionic compounds K[Ni(cAAC^{Me}-CS$_2$)$_2$] (**4a^K**) and K[Ni(IDipp-CS$_2$)$_2$] (**4b^K**) these absorptions vanish. Instead, **4a^K** and **4b^K** display

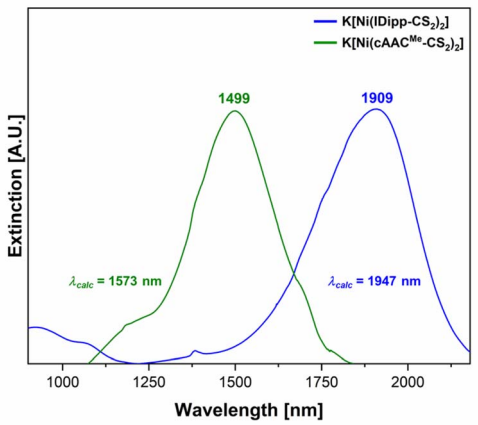

Fig. 10 Experimental UV/VIS/NIR absorption spectra of K[Ni(cAAC^{Me}-CS$_2$)$_2$] (**4a^K**, green) and K[Ni(IDipp-CS$_2$)$_2$] (**4b^K**, blue) in THF in the NIR region and TD-DFT (PBE0-D3BJ//def2-TZVPP(Ni)/def2-TZVP(C,H,N,S)/COSMO(THF)) calculated absorption maxima λ_{calc}.

significantly red shifted broad NIR-absorptions at wavelengths of 1499 nm for **4a^K** and at even lower energies for **4b^K**, which absorbs at 1909 nm. These absorption maxima are in line with TD-DFT calculations (PBE0-D3BJ//def2-TZVPP(Ni)/def2-TZVP(C,H,N,S)/COSMO(THF)) performed on [Ni(cAAC^{Me}-CS$_2$)$_2$]$^{\cdot-}$ (**4a**) and [Ni(IDipp-CS$_2$)$_2$]$^{\cdot-}$ (**4b**), which predict characteristic intense absorptions (λ_{calc}) of these metalates at 1573 nm (**4a**) and 1947 nm (**4b**) (see Fig. S9 of the ESI‡). These absorptions are shifted to higher energies compared to the neutral nickel complexes **3a** (λ_{calc} = 1008 nm) and **3b** (λ_{calc} = 1034 nm) and are due to electronic transitions between the doubly occupied π_1 orbital and the singly occupied π_2 orbital, *i.e.* $\pi_1(\beta) \rightarrow \pi_2(\beta)$, and are thus essentially IVCT bands.

The observed drastic differences in the NIR-absorptions of **4a^K** and **4b^K** demonstrate that small changes in the carbene-CS$_2$ scaffold strongly influence the absorption spectra of these reduced nickelates, which allows tuning of the redox state dependent NIR absorptivity in these systems by substitutional variation. These basic observations may lay the foundation for further development towards application of such nickel bis-(carbene-CS$_2$) complexes as tunable and switchable electrochromic NIR dyes, enabled by the distinct redox activity of carbene-CS$_2$ ligands.

Conclusions

In this study we demonstrated that azolium-2-dithiocarboxylates are redox active ligands in nickel complexes and that the redox activity of these carbene-CS$_2$ adducts enables access to a variety of formal ligand based redox states. Using nickel(0) precursors and depending on other ancillary co-ligands, bonding of carbene-CS$_2$ adducts through κ^2-*S*,*S*′ coordination led to the formation of mono- or bis-(carbene-CS$_2$) complexes of the types [NiL$_2$(carbene-CS$_2$)] (**2a–g**) or [Ni(carbene-CS$_2$)$_2$] (**3a–c**), in which the ligands were reduced upon coordination to the central nickel atom. Reduction by external redox reagents afforded anionic nickelates [Ni(carbene-CS$_2$)$_2$]$^{\cdot-}$ (**4a–b^K**). The ligand redox states in these compounds range from radical monoanionic (Scheme 2; **B**: **3a–c**) and dianionic (Scheme 2; **C**: **2a–g**) to a redox state with a non-integer negative charge of −1.5 (**4a–b^K**). SC-XRD analytic evaluation of the structural parameters such as C$_{Carbene}$–C$_{CS2}$, C–N, and C–S distances or ∡NCCS torsion angles of the ligated carbene-CS$_2$ adducts proved that these parameters are valuable tools for the determination of the ligands' redox state and thus also for the evaluation of the formal oxidation state of the central nickel atom, which in this study was exclusively Ni(II). Moreover, the strong electronic coupling of the two radical anionic carbene-CS$_2$ ligands in the homoleptic complexes **3a–c** led to the description of the electronic structure as a singlet diradical with admixtures from a triplet state that is only slightly higher in energy, which was indicated by quantum chemical calculations and also experimentally corroborated by the diamagnetic character of the ligands in these complexes, except for the central C$_{Carbene}$ and C$_{CS2}$ carbon atoms, as well as by the presence of characteristic intense ligand-to-ligand charge transfer (LLCT) transitions in the NIR region of their electronic

absorption spectra at 1076 nm (**3a**), 1077 nm (**3b**) and 1064 nm (**3c**). In the nickelates **4a–b^{K}** the added electron is equally delocalized across the π-system of both carbene-CS_2 ligands, leading to a ligand-based mixed-valent (LBMV) redox-state corresponding to the Robin-Day class III. Consequently, these nickelates exhibit characteristic IVCT transitions, which are strongly red-shifted relative to those of **3a–c**, with experimental values of 1499 nm (**4a^{K}**) and 1909 nm (**4b^{K}**). This work lays the foundation to understand the interesting chemical reactivity and physical properties of redox-active carbene-CS_2 ligands in general and of their transition metal complexes and thus paves the way for the application of azolium-2-dithiocarboxylate ligands in different applications, for example, as redox catalysts, as electronically switchable materials or as NIR dyes.

Data availability

The data supporting this article have been included as ESI.‡ Crystallographic data (excluding structure factors) for the structures in this paper have been deposited with the Cambridge Crystallographic Data Centre, CCDC, 12 Union Road, Cambridge CB21EZ, UK.

Author contributions

M. S. L. and U. R. conceived of the project; M. S. L., T. M. F. and C. S. C. conducted most of the experiments, K. O. performed CV analyses, I. K. performed EPR spectroscopy, U. R. carried out quantum-chemical calculations, and R. B. conducted solid-state NMR spectroscopy; M. S. L., U. R., M. F., and H. B. wrote the manuscript.

Conflicts of interest

The authors declare no conflict of interest.

Acknowledgements

This work was supported by funds from the Julius-Maximilians-Universität Würzburg.

References

1 (*a*) P. J. Chirik, *Inorg. Chem.*, 2011, **50**, 9737–9740; (*b*) V. Lyaskovskyy and B. de Bruin, *ACS Catal.*, 2012, **2**, 270–279; (*c*) V. K. K. Praneeth, M. R. Ringenberg and T. R. Ward, *Angew. Chem. Int. Ed.*, 2012, **51**, 10228–10234; *Angew. Chem.*, 2012, **124**, 10374–10380; (*d*) J. R. Khusnutdinova and D. Milstein, *Angew. Chem. Int. Ed.*, 2015, **54**, 12236–12273; *Angew. Chem.*, 2015, **127**, 12406–12445; (*e*) M. R. Elsby and R. T. Baker, *Chem. Soc. Rev.*, 2020, **49**, 8933–8987; (*f*) A. Nakada, T. Matsumoto and H.-C. Chang, *Coord. Chem. Rev.*, 2022, **473**, 214804; (*g*) S. B. H. Karnbrock and M. Alcarazo, *Chem.–Eur. J.*, 2024, **30**, e202302879; (*h*) *Redox-Active Ligands. Concepts and Catalysis*, ed. M. Desage-El Murr, Wiley-VCh, Weinheim, 2024.

2 U. Rastetter, A. Jacobi von Wangelin and C. Herrmann, *J. Comput. Chem.*, 2023, **44**, 468–479.

3 G. G. Briand, *Dalton Trans.*, 2023, **52**, 17666–17678.

4 R. Mondal, A. K. Guin, G. Chakraborty and N. D. Paul, *Org. Biomol. Chem.*, 2022, **20**, 296–328.

5 (*a*) B. Singh and A. Indra, *Inorg. Chim. Acta*, 2020, **506**, 119440; (*b*) T. Benkó, D. Lukács, M. Li and J. S. Pap, *Environ. Chem. Lett.*, 2022, **20**, 3657–3695.

6 C. K. Prier, D. A. Rankic and D. W. C. MacMillan, *Chem. Rev.*, 2013, **113**, 5322–5363.

7 (*a*) O. R. Luca and R. H. Crabtree, *Chem. Soc. Rev.*, 2013, **42**, 1440–1459; (*b*) Z. Niu, L. Yang, Y. Xiao, M. Xue, J. Zhou, L. Zhang, J. Zhang, D. P. Wilkinson and C. Ni, *Electrocatalysis*, 2022, **13**, 230–241.

8 A. Hinz, J. Bresnien, F. Breher and A. Schulz, *Chem. Rev.*, 2023, **123**, 10468–10526.

9 (*a*) J. A. McCleverty, *Prog. Inorg. Chem.*, 1968, **10**, 49–221; (*b*) R. Eisenberg, *Coord. Chem. Rev.*, 2011, **255**, 825–836; (*c*) R. Eisenberg and H. B. Gray, *Inorg. Chem.*, 2011, **50**, 9741–9751.

10 (*a*) C. K. Jørgensen, *Coord. Chem. Rev.*, 1966, **1**, 164–178; (*b*) M. D. Ward and J. A. McCleverty, *J. Chem. Soc., Dalton Trans.*, 2002, 275–288.

11 (*a*) F. Bigoli, P. Deplano, F. A. Devillanova, J. R. Ferraro, V. Lippolis, P. J. Lukes, M. L. Mercuri, M. A. Pellinghelli, E. F. Trogu and J. M. Williams, *Inorg. Chem.*, 1997, **36**, 1218–1226; (*b*) *Dithiolene Chemistry: Synthesis, Properties, and Applications*, ed. E. I. Stiefel, John Wiley & Sons, Hoboken, New Jersey, 2004, vol. 52; (*c*) P. Deplano, L. Pilia, D. Espa, M. L. Mercuri and A. Serpe, *Coord. Chem. Rev.*, 2010, **254**, 1434–1447; (*d*) B. Garreau-de Bonneval, K. I. Moineau-Chane Ching, F. Alary, T.-T. Bui and L. Valade, *Coord. Chem. Rev.*, 2010, **254**, 1457–1467.

12 (*a*) U. T. Mueller-Westerhoff, B. Vance and D. I. Yoon, *Tetrahedron*, 1991, **47**, 909–932; (*b*) P. Deplano, M. L. Mercuri, G. Pintus and E. F. Trogu, *Comments Inorg. Chem.*, 2001, **22**, 353–374; (*c*) D. Natali, M. Sampietro, M. Arca, C. Denotti and F. A. Devillanova, *Synth. Met.*, 2003, **137**, 1489–1490; (*d*) M. Caironi, D. Natali, M. Sampietro, M. Ward, A. Meacham, F. A. Devillanova, M. Arca, C. Denotti and L. Pala, *Synth. Met.*, 2005, **153**, 273–276; (*e*) M. C. Aragoni, M. Arca, F. A. Devillanova, F. Isaia, V. Lippolis, A. Mancini, L. Pala, G. Verani, T. Agostinelli, M. Caironi, D. Natali and M. Sampietro, *Inorg. Chem. Commun.*, 2007, **10**, 191–194; (*f*) Y. Liu, Z. Zhang, X. Chen, S. Xu and S. Cao, *Dyes Pigm.*, 2016, **128**, 179–189; (*g*) F. Camerel and M. Fourmigué, *Eur. J. Inorg. Chem.*, 2020, 508–522; (*h*) K. Chen, W. Fang, Q. Zhang, X. Jiang, Y. Chen, W. Xu, Q. Shen, P. Sun and W. Huang, *ACS Appl. Bio Mater.*, 2021, **4**, 4406–4412.

13 (*a*) J. P. Fackler and D. Coucouvanis, *Chem. Commun.*, 1965, 556–557; (*b*) J. P. Fackler, Jr. and D. Coucouvanis, *J. Am. Chem. Soc.*, 1966, **88**, 3913–3920; (*c*) D. Coucouvanis, *Prog. Inorg. Chem.*, 1970, 233–371; (*d*) F. J. Hollander, M. L. Caffery and D. Coucouvanis, *J. Am. Chem. Soc.*, 1974, **96**, 4682–4684; (*e*) D. Coucouvanis, F. J. Hollander and M. L. Caffery, *Inorg. Chem.*, 1976, **15**, 1853–1860; (*f*)

S. Sproules, C. I. Macleod, O. D. Keramidas and H. N. Miras, *Chem.–Eur. J.*, 2024, **30**, e202401710.

14 (*a*) H. E. Winberg and D. D. Coffman, *J. Am. Chem. Soc.*, 1965, **87**, 2776–2777; (*b*) W. S. Sheldrick, A. Schönberg, E. Singer and P. Eckert, *Chem. Ber.*, 1980, **113**, 3605–3609; (*c*) W. Krasuski, D. Nikolaus and M. Regitz, *Liebigs Ann. Chem.*, 1982, 1451–1465; (*d*) N. Kuhn, H. Bohnen and G. Henkel, *Z. Naturforsch., B*, 1994, **49**, 1473–1480; (*e*) J. Nakayama, T. Kitahara, Y. Sugihara, A. Sakamoto and A. Ishii, *J. Am. Chem. Soc.*, 2000, **122**, 9120–9126; (*f*) G. Kuchenbeiser, M. Soleilhavoup, B. Donnadieu and G. Bertrand, *Chem.–Asian J.*, 2009, **4**, 1745–1750; (*g*) L. Delaude, *Eur. J. Inorg. Chem.*, 2009, 1681–1699; (*h*) L. Delaude, A. Demonceau and J. Wouters, *Eur. J. Inorg. Chem.*, 2009, 1882–1891; (*i*) A. R. Katritzky, D. Jishkariani, R. Sakhuja, C. D. Hall and P. J. Steel, *J. Org. Chem.*, 2011, **76**, 4082–4087; (*j*) U. Siemeling, H. Memczak, C. Bruhn, F. Vogel, F. Träger, J. E. Baio and T. Weidner, *Dalton Trans.*, 2012, **41**, 2986–2994; (*k*) T. F. Beltrán, G. Zaragoza and L. Delaude, *Dalton Trans.*, 2017, **46**, 9036–9048; (*l*) F. Mazars, M. Hrubaru, N. Tumanov, J. Wouters and L. Delaude, *Eur. J. Org Chem.*, 2021, 2025–2033; (*m*) N. Touj, F. Mazars, G. Zaragoza and L. Delaude, *Beilstein J. Org. Chem.*, 2023, **19**, 1947–1956.

15 (*a*) L. L. Borer, J. Kong and E. Sinn, *Inorg. Chim. Acta*, 1986, **122**, 145–148; (*b*) T. Fujihara, T. Sugaya, A. Nagasawa and J. Nakayama, *Acta Cryst. Sect. E*, 2004, **60**, m282–m284; (*c*) L. Delaude, X. Sauvage, A. Demonceau and J. Wouters, *Organometallics*, 2009, **28**, 4056–4064; (*d*) T. Sugaya, T. Fujihara, A. Nagasawa and K. Unoura, *Inorg. Chim. Acta*, 2009, **362**, 4813–4822; (*e*) S. Naeem, L. Delaude, A. J. P. White and J. D. E. T. Wilton-Ely, *Inorg. Chem.*, 2010, **49**, 1784–1793; (*f*) S. Naeem, A. L. Thompson, L. Delaude and J. D. E. T. Wilton-Ely, *Chem.–Eur. J.*, 2010, **16**, 10971–10974; (*g*) S. Naeem, A. L. Thompson, A. J. P. White, L. Delaude and J. D. E. T. Wilton-Ely, *Dalton Trans.*, 2011, **40**, 3737–3747; (*h*) M. J. D. Champion, R. Solanki, L. Delaude, A. J. P. White and J. D. E. T. Wilton-Ely, *Dalton Trans.*, 2012, **41**, 12386–12394; (*i*) A. Neuba, J. Ortmeyer, D. D. Konieczna, G. Weigel, U. Flörke, G. Henkel and R. Wilhelm, *RSC Adv.*, 2015, **5**, 9217–9220; (*j*) T. F. Beltrán, G. Zaragoza and L. Delaude, *Dalton Trans.*, 2016, **45**, 18346–18355; (*k*) T. F. Beltrán, G. Zaragoza and L. Delaude, *Dalton Trans.*, 2017, **46**, 1779–1788; (*l*) T. F. Beltrán, G. Zaragoza and L. Delaude, *Dalton Trans.*, 2017, **46**, 13002–13009; (*m*) J. Ortmeyer, U. Flörke, G. Henkel, R. Wilhelm and A. Neuba, *Eur. J. Inorg. Chem.*, 2017, 3191–3197; (*n*) T. F. Beltrán, G. Zaragoza and L. Delaude, *Polyhedron*, 2021, **197**, 115055; (*o*) P. Rungthanaphatsophon, A. J. Gremillion, Y. Wang, S. P. Kelley, G. H. Robinson and J. R. Walensky, *Inorg. Chim. Acta*, 2021, **514**, 120033; (*p*) P. Pérez-Ramos, M. A. Mateo, D. Elorriaga, D. García-Vivó, R. G. Soengas and H. Rodríguez-Solla, *Dalton Trans.*, 2024, **53**, 9433–9440; (*q*) V. P. Carvalho, G. Zaragoza and L. Delaude, *Dalton Trans.*, 2024, **53**, 11436–11444; (*r*) F. Mazars, G. Zaragoza and L. Delaude, *Organometallics*, 2024, **43**, 2284–2304; (*s*) S. Park, J.-Y. Hwang, J. Shin and Y. Kim, *J. Am. Chem. Soc.*, 2024, **146**, 28508–28515; (*t*) M. Lee, H. Noh and Y. Kim, *Chem. Commun.*, 2024, **60**, 13867–13870.

16 M. S. Luff, I. Krummenacher, K. Oppel, H. Braunschweig and U. Radius, *Chem. Commun.*, 2024, **60**, 14447–14450.

17 N. Kuhn, G. Weyers and G. Henkel, *Chem. Commun.*, 1997, 627–628.

18 The X-ray structure of this compound, however, is reported, see P. G. Jones and I. Dix, *CSD Commun.*, 2004, CCDC: 238439.

19 (*a*) T. Schaub and U. Radius, *Z. Anorg. Allg. Chem.*, 2006, **632**, 807–813; (*b*) T. Schaub and U. Radius, *Z. Anorg. Allg. Chem.*, 2006, **632**, 981–984; (*c*) U. Radius and F. M. Bickelhaupt, *Organometallics*, 2008, **27**, 3410–3414; (*d*) T. Schaub, P. Fischer, T. Meins and U. Radius, *Eur. J. Inorg. Chem.*, 2011, 3122–3126; (*e*) T. Zell, P. Fischer, D. Schmidt and U. Radius, *Organometallics*, 2012, **31**, 5065–5073; (*f*) D. Schmidt, T. Zell, T. Schaub and U. Radius, *Dalton Trans.*, 2014, **43**, 10816–10827; (*g*) M. W. Kuntze-Fechner, H. Verplancke, L. Tendera, M. Diefenbach, I. Krummenacher, H. Braunschweig, T. B. Marder, M. C. Holthausen and U. Radius, *Chem. Sci.*, 2020, **11**, 11009–11023; (*h*) L. Tendera, M. Helm, M. J. Krahfuss, M. W. Kuntze-Fechner and U. Radius, *Chem.–Eur. J.*, 2021, **27**, 17849–17861; (*i*) L. Tendera, M. S. Luff, I. Krummenacher and U. Radius, *Eur. J. Inorg. Chem.*, 2022, e202200416; (*j*) L. Tendera, F. Fantuzzi, T. B. Marder and U. Radius, *Chem. Sci.*, 2023, **14**, 2215–2228; (*k*) L. Tendera, L. Kuehn, T. B. Marder and U. Radius, *Chem.–Eur. J.*, 2023, **29**, e202302310; (*l*) M. S. Luff, C. Kerpen, J. A. P. Sprenger, M. Finze and U. Radius, *Inorg. Chem.*, 2024, **63**, 2204–2216; (*m*) M. S. Luff, L. Walther, M. Finze and U. Radius, *Dalton Trans.*, 2024, **53**, 5391–5400.

20 (*a*) T. Schaub and U. Radius, *Chem.–Eur. J.*, 2005, **11**, 5024–5030; (*b*) P. Fischer, T. Linder and U. Radius, *Z. Anorg. Allg. Chem.*, 2012, **638**, 1491–1496; (*c*) J. H. J. Berthel, L. Tendera, M. W. Kuntze-Fechner, L. Kuehn and U. Radius, *Eur. J. Inorg. Chem.*, 2019, 3061–3072; (*d*) L. Kuehn, D. G. Jammal, K. Lubitz, T. B. Marder and U. Radius, *Chem.–Eur. J.*, 2019, **25**, 9514–9521; (*e*) J. H. J. Berthel, M. J. Krahfuß and U. Radius, *Z. Anorg. Allg. Chem.*, 2020, **646**, 692–704.

21 Anamika, D. K. Yadav, K. K. Manar, C. L. Yadav, K. Kumar, V. Ganesan, M. G. B. Drew and N. Singh, *Dalton Trans.*, 2020, **49**, 3592–3605.

22 (*a*) L. A. Freeman, A. D. Obi, H. R. Machost, A. Molino, A. W. Nichols, D. A. Dickie, D. J. D. Wilson, C. W. Machan and R. J. Gilliard, *Chem. Sci.*, 2021, **12**, 3544–3550; (*b*) N. Kuhn, G. Weyers, S. Dümmling and B. Speiser, *Phosphorus Sulfur Silicon Relat. Elem.*, 1997, **128**, 45–62.

23 G. J. Martin, J. P. Gouesnard, J. Dorie, C. Rabiller and M. L. Martin, *J. Am. Chem. Soc.*, 1977, **99**, 1381–1384.

24 F. H. Allen, O. Kennard, D. G. Watson, L. Brammer, A. G. Orpen and R. Taylor, *J. Chem. Soc. Perk. Trans.*, 1987, **2**, S1–S19.

25 (*a*) B. S. Lim, D. V. Fomitchev and R. H. Holm, *Inorg. Chem.*, 2001, **40**, 4257–4262; (*b*) M. C. Aragoni, C. Caltagirone,

V. Lippolis, E. Podda, A. M. Z. Slawin, J. D. Woollins, A. Pintus and M. Arca, *Inorg. Chem.*, 2020, **59**, 17385–17401; (*c*) Z. M. Wong, X. Yong, T. Deng, W. Shi, G. Wu, N. Li, H.-K. Luo and S.-W. Yang, *J. Phys. Chem. A*, 2022, **126**, 5552–5558; (*d*) K. Youssef, C. Poidevin, A. Vacher, A. Fihey, Y. Le Gal, T. Roisnel and D. Lorcy, *Dalton Trans.*, 2024, **53**, 9763–9776.

26 (*a*) U. S. D. Paul and U. Radius, *Eur. J. Inorg. Chem.*, 2017, 3362–3375; (*b*) U. S. D. Paul and U. Radius, *Organometallics*, 2017, **36**, 1398–1407; (*c*) U. S. D. Paul, M. J. Krahfuß and U. Radius, *Chem. unserer Zeit*, 2019, **53**, 212–223.

27 (*a*) M. B. Robin and P. Day, *Adv. Inorg. Chem. Radiochem.*, 1968, **10**, 247–422; (*b*) A. Vogler and H. Kunkely, *Comments Inorg. Chem.*, 1990, **9**, 201–220; (*c*) A. Vogler and H. Kunkely, *Coord. Chem. Rev.*, 2007, **251**, 577–583.

28 (*a*) M. M. Roessler and E. Salvadori, *Chem. Soc. Rev.*, 2018, **47**, 2534–2553; (*b*) M. Ju, J. Kim and J. Shin, *Bull. Korean Chem. Soc.*, 2024, **45**, 835–862.